Three-neutrino mixing after the first results from K2K and KamLAND

M. C. Gonzalez-Garcia*
YITP, SUNY at Stony Brook, Stony Brook, New York 11794-3840, USA
and IFIC, Universitat de València–CSIC, Apt 22085, 46071 València, Spain

Carlos Peña-Garay†
School of Natural Sciences, Institute for Advanced Study, Princeton, New Jersey 08540, USA
(Received 9 June 2003; published 11 November 2003)

We analyze the impact of the data on long-baseline ν_μ disappearance from the K2K experiment and reactor $\bar{\nu}_e$ disappearance from the KamLAND experiment on the determination of the leptonic three-generation mixing parameters. Performing an up-to-date global analysis of solar, atmospheric, reactor, and long-baseline neutrino data in the context of three-neutrino oscillations, we determine the presently allowed ranges of masses and mixing and we consistently derive the allowed magnitude of the elements of the leptonic mixing matrix. We also quantify the maximum allowed contribution of Δm^2_{21} oscillations to *CP*-odd and *CP*-even observables at future long-baseline experiments.

DOI: 10.1103/PhysRevD.68.093003 PACS number(s): 14.60.Pq, 12.15.Ff, 26.65.+t

I. INTRODUCTION

Neutrino oscillations are entering a new era in which the observations from underground experiments obtained with neutrino beams provided to us by nature—either from the Sun or from the interactions of cosmic rays in the upper atmosphere—are being confirmed by experiments using ''manmade'' neutrinos from accelerators and nuclear reactors.

Super-Kamiokande (SK) high statistics data [1,2] clearly established that the observed deficit in the μ-like atmospheric events is due to neutrinos arriving in the detector at large zenith angles, strongly suggestive of the ν_μ oscillation hypothesis. This evidence was also confirmed by other atmospheric experiments such as MACRO [3] and Soudan 2 [4]. Similarly, the SNO results [5] in combination with the SK data on the zenith angle dependence and recoil energy spectrum of solar neutrinos [6] and the Homestake [7], SAGE [8], GALLEX+GNO [9,10], and Kamiokande [11] experiments put on a firm observational basis the long-standing problem of solar neutrinos [12], establishing the need for ν_e conversions.

The KEK to Kamioka long-baseline neutrino oscillation experiment (K2K) uses an accelerator-produced neutrino beam mostly consisting of ν_μ with a mean energy of 1.3 GeV and a neutrino flight distance of 250 km to probe the same oscillations that were explored with atmospheric neutrinos. Their results [13] show that both the number of observed neutrino events and the observed energy spectrum are consistent with neutrino oscillations with oscillation parameters consistent with the ones suggested by atmospheric neutrinos.

The KamLAND experiment measures the flux of $\bar{\nu}_e$'s from nuclear reactors with an energy of $\sim$MeV located at a typical distance of $\sim$180 km with the aim of exploring with a terrestrial beam the region of neutrino parameters that is relevant for the oscillation interpretation of the solar data. Their first published [14] results show that both the total number of events and their energy spectrum can be better interpreted in terms of $\bar{\nu}_e$ oscillations with parameters consistent with the large merging angle (LMA) solar neutrino solution [14–17].

Altogether, the data from solar and atmospheric neutrino experiments and the first results from KamLAND and K2K constitute the only solid present-day evidence for physics beyond the standard model [18]. The minimum joint description of these data requires neutrino mixing among all three known neutrinos and it determines the structure of the lepton mixing matrix [19], which can be parametrized as [20]

$$U=\begin{pmatrix} c_{13}c_{12} & s_{12}c_{13} & s_{13}e^{-i\delta} \\ -s_{12}c_{23}-s_{23}s_{13}c_{12}e^{i\delta} & c_{23}c_{12}-s_{23}s_{13}s_{12}e^{i\delta} & s_{23}c_{13} \\ s_{23}s_{12}-s_{13}c_{23}c_{12}e^{i\delta} & -s_{23}c_{12}-s_{13}s_{12}c_{23}e^{i\delta} & c_{23}c_{13} \end{pmatrix}, \quad (1)$$

*Email address: concha@insti.physics.sunysb.edu
†Email address: penya@ias.edu

where $c_{ij} \equiv \cos\theta_{ij}$ and $s_{ij} \equiv \sin\theta_{ij}$. In addition to the Dirac-type phase δ analogous to that of the quark sector, there are two physical phases associated with the Majorana character of neutrinos, which, however, are not relevant for neutrino oscillations [21] and will be set to zero in what follows.

In this paper we present the result of a global analysis of solar, atmospheric, reactor, and long-baseline neutrino data in the context of three-neutrino oscillations with the aim of determining in a consistent way our present knowledge of the leptonic mixing matrix and the neutrino mass differences. We place particular emphasis on the impact of the first data from long-baseline ν_μ disappearance from the K2K experiment and reactor $\bar{\nu}_e$ disappearance from the KamLAND experiment.

The outline of the paper is as follows. In Sec. II we describe the data included in the analysis and briefly describe the relevant formalism. Section III A contains the results of the analysis of the K2K data and their effect on the determination of the parameters associated with atmospheric oscillations. We find that the main impact of K2K when combined with atmospheric neutrino data is to reduce the allowed range of the corresponding mass difference. When combined with the data from the CHOOZ [22] experiment in a three-neutrino analysis, this results in a slight tightening of the derived bound on θ_{13} at high C.L. In Sec. III B we describe the results from the global analysis including also solar and KamLAND data, and in Sec. III C we describe our procedure to consistently derive the allowed magnitude of the elements of the leptonic mixing matrix. As an outcome of this analysis we also quantify the maximum allowed contribution of Δm^2_{21} oscillations to *CP*-odd and *CP*-even observables at future long-baseline experiments in Sec. III D. Conclusions are given in Sec. IV. We also present an Appendix with the details of our analysis of the K2K data.

II. DATA INPUTS AND FORMALISM

We include in our statistical analysis the data from solar, atmospheric, and K2K accelerator neutrinos and from the CHOOZ and KamLAND reactor antineutrinos.

In the analysis of K2K we include the data on the normalization and shape of the spectrum of single-ring μ-like events as a function of the reconstructed neutrino energy. The total sample corresponds to 29 events. In the absence of oscillations, 44 events were expected. We bin the data in five 0.5 GeV bins with $0 < E_{\rm rec} < 2.5$ plus one bin containing all events above 2.5 GeV. For quasielastic (QE) events the reconstructed neutrino energy is well distributed around the true neutrino energy. However, experimental energy and angular resolution and more importantly the contamination from non-QE events result in important deviations of the reconstructed neutrino energy from the true neutrino energy, which we carefully account for. We include the systematic uncertainties associated with the determination of the neutrino energy spectrum in the near detector, the model dependence of the amount of non-QE contamination, the near/far extrapolation, and the overall flux normalization. Details of this analysis are presented in the Appendix.

For atmospheric neutrinos we include in our analysis all the contained events from the latest 1489 SK data set [1], as well as the upward-going neutrino-induced muon fluxes from both SK and the MACRO detector [3]. This amounts to a total of 65 data points. A more technical description of our simulations and statistical analysis can be found in Refs. [23,24].

We refine our previous analysis [24,25] of the CHOOZ reactor data [22] and include here their energy binned data instead of their total rate only. This corresponds to 14 data points (seven-bin positron spectra from both reactors, Table 4 in Ref. [22]) with one constrained normalization parameter and including all the systematic uncertainties there described.

For the solar neutrino analysis, we use 80 data points. We include the two measured radiochemical rates, from the chlorine [7] and the gallium [8–10] experiments, the 44 zenith-spectral energy bins of the electron neutrino scattering signal measured by the SK Collaboration [6], and the 34 day-night spectral energy bins measured with the SNO [5] detector. We take account of the BP00 [26] predicted fluxes and uncertainties for all solar neutrino sources except for ^{8}B neutrinos. We treat the total ^{8}B solar neutrino flux as a free parameter to be determined by experiment and to be compared with solar model predictions. For KamLAND we include information on the observed antineutrino spectrum which accounts for a total of 13 data points. Details of our calculations and statistical treatment of solar and KamLAND data can be found in Refs. [15,16].

In general, the parameter set relevant for the joint study of these neutrino data in the framework of three-ν mixing is six dimensional: two mass differences, three mixing angles, and one *CP* phase.

Results from the analysis of solar plus KamLAND and atmospheric data in the framework of oscillations between two neutrino states [15–17,23,27] imply that the required mass differences satisfy

$$\Delta m^2_\odot \ll \Delta m^2_{\rm atm}. \tag{2}$$

In this approximation, the angles θ_{ij} in Eq. (1) can be taken without loss of generality to lie in the first quadrant, $\theta_{ij} \in [0, \pi/2]$. There are two possible mass orderings, which we chose as

$$\Delta m^2_{21} = \Delta m^2_\odot \ll \Delta m^2_{32} \simeq \Delta m^2_{31} = \Delta m^2_{\rm atm} > 0; \tag{3}$$

$$\Delta m^2_{21} = \Delta m^2_\odot \ll -\Delta m^2_{31} \simeq -\Delta m^2_{32} = |\Delta m^2_{\rm atm}| > 0. \tag{4}$$

As is customary we refer to the first option, Eq. (3), as the *normal* scheme, and to the second one, Eq. (4), as the *inverted* scheme.

For solar neutrinos and for antineutrinos in KamLAND the oscillations with $\Delta m^2_{32} \sim \Delta m^2_{31}$ are averaged out. The relevant survival probability takes the form

$$P^{3\nu}_{ee} = \sin^4\theta_{13} + \cos^4\theta_{13} P^{2\nu}_{ee}(\Delta m^2_{21}, \theta_{12}), \tag{5}$$

where $P^{2\nu}_{ee}(\Delta m^2_{21}, \theta_{12})$ is the survival probability for $2\,\nu$ mixing, which, for solar neutrinos, is obtained with the modified sun density $N_e \to \cos^2\theta_{13} N_e$. So the analysis of solar and

KamLAND data depends on three of the five oscillation parameters: Δm^2_{21}, θ_{12}, and θ_{13}.

Conversely, for small Δm^2_{21} the three-neutrino oscillation analysis of the atmospheric and K2K neutrino data can be performed in the one-mass-scale dominance approximation, neglecting the effect of Δm^2_{21}. In this approximation the angle θ_{12} can be rotated away, and it follows that the atmospheric and K2K data analysis restricts three of the oscillation parameters, namely, $\Delta m^2_{31}=\Delta m^2_{32}$, θ_{23}, and θ_{13}, and the *CP* phase δ becomes unobservable. The ν_μ survival probability at K2K is

$$P^{\rm K2K}_{\mu\mu}=1-4(s^4_{23}s^2_{13}c^2_{13}+c^2_{13}s^2_{23}c^2_{23})\sin^2\left(\frac{\Delta m^2_{32}}{4E_\nu}L\right)$$
$$\simeq s^2_{13}\frac{\cos 2\theta_{23}}{c^2_{23}}+\left(1-s^2_{13}\frac{\cos 2\theta_{23}}{c^2_{23}}\right)\times P^{K2K,2\nu}_{\mu\mu}(\Delta m^2_{32},\theta_{32})+\mathcal{O}(s^4_{13}). \quad (6)$$

For atmospheric neutrinos in the general case of the three-neutrino scenario with $\theta_{13}\neq 0$, the presence of the matter potentials becomes relevant. We solve numerically the evolution equations in order to obtain the oscillation probabilities for both e and μ flavors, which are different for neutrinos and antineutrinos. Because of the matter effects, they also depend on the mass ordering being normal or inverted. In our calculations, we use for the matter density profile of the Earth the approximate analytic parametrization given in Ref. [28] of the PREM (preliminary reference Earth model) of the Earth [29].

The reactor neutrino data from CHOOZ provide information on the survival probability [24,30,31]:

$$P^{\rm CHOOZ}_{ee}=1-c^4_{13}\sin^2 2\theta_{12}\sin^2\left(\frac{\Delta m^2_{21}L}{4E_\nu}\right)-\sin^2 2\theta_{13}\left[c^2_{12}\sin^2\left(\frac{\Delta m^2_{31}L}{4E_\nu}\right)+s^2_{12}\sin^2\left(\frac{\Delta m^2_{32}L}{4E_\nu}\right)\right]$$
$$\simeq 1-\sin^2 2\theta_{13}\sin^2\left(\frac{\Delta m^2_{32}L}{4E_\nu}\right). \quad (7)$$

The second equality holds in the approximation $\Delta m^2_{21}\ll E_\nu/L$, which can be safely made for the presently allowed values of Δm^2_{21} [16,17]. Thus the analysis of the CHOOZ reactor data involves only two parameters: Δm^2_{32} and the mixing angle θ_{13}.

In summary, oscillations in solar+KamLAND data on one side, and atmospheric+K2K oscillations on the other side, decouple in the limit $\theta_{13}=0$. In this case the values of the allowed parameters can be obtained directly from the results of the analysis in terms of two-neutrino oscillations, and the normal and inverted hierarchies are equivalent. Deviations from the two-neutrino scenario are determined by the size of the mixing θ_{13}.

The allowed ranges of masses and mixing obtained in our two-neutrino oscillation analysis of solar+KamLAND data can be found in Ref. [16], and we do not reproduce them here. We discuss next the results of our analysis of K2K data and its impact on the determination of the parameters relevant in atmospheric oscillations.

III. RESULTS

A. Δm^2_{32} oscillations: Impact of K2K data

For the sake of comparison with the K2K oscillation analysis, we discuss first the results of our analysis of K2K data for pure $\nu_\mu\to\nu_\tau$ oscillations, which are graphically displayed in Fig. 1.

We show in the left panel of Fig. 1 the allowed region of $(\Delta m^2,\sin^2(2\theta))$ from our analysis of K2K data. The best fit point for this analysis is at $\Delta m^2=2.7\times10^{-3}$ eV^2, $\sin^2(2\theta)=0.92$ with $\chi^2_{\rm min}=9.3$ [the corresponding best fit as obtained from the K2K Collaboration is at $\Delta m^2=2.7\times10^{-3}$ eV^2, $\sin^2(2\theta)=1$]. We notice that the nonmaximality of the mixing angle in our analysis is not statistically significant as maximal mixing occurs only at $\Delta\chi^2=0.15$. The energy spectrum for this point is shown in the right panel together with the data points and the expectations in the absence of oscillations. Our results show very good agreement with those obtained by the K2K Collaboration [13]. Also displayed in the figure are the corresponding regions from our latest atmospheric neutrino analysis [25]. As seen in the figure, the K2K results confirm the presence of ν_μ neutrino oscillations with oscillation parameters consistent with the ones obtained from atmospheric neutrino studies. Furthermore, already at this first stage, the results provide a restriction on the allowed range of Δm^2, while their dependence on the mixing angle is considerably weaker.

In the framework of 3ν mixing, the analysis of K2K, atmospheric, and CHOOZ data provides information on the parameters Δm^2_{31}, θ_{23}, and θ_{13}. We define

$$\chi^2_{\rm atm+CHOOZ+K2K}(\Delta m^2_{32},\theta_{23},\theta_{13})=\chi^2_{\rm atm}(\Delta m^2_{32},\theta_{23},\theta_{13})+\chi^2_{\rm CHOOZ}(\Delta m^2_{32},\theta_{13})+\chi^2_{\rm K2K}(\Delta m^2_{32},\theta_{23},\theta_{13}). \quad (8)$$

In the three panels of Fig. 2 we show the bounds on each of the three parameters obtained from this analysis (full lines). For comparison we also show the corresponding ranges for the analysis of atmospheric and CHOOZ data alone (dotted lines). The corresponding subtracted minima are given in Table I. The results in the figure are shown for the normal mass ordering, but once the constraint on θ_{13} from CHOOZ is included in the analysis, the differences between the results for normal and inverted mass ordering are minimal. The careful reader may notice that the χ^2 per DOF seems *too good*. As seen in Table I this effect is driven by the atmospheric data and it was already the case for the previous SK data sample. It is partly due to the very good agreement of the multi-GeV electron distributions with their no-oscillation expectations. However, as discussed in Ref. [32], $\chi^2_{\rm min}$ is only 2σ below its characteristic value, not low enough to be statistically suspected.

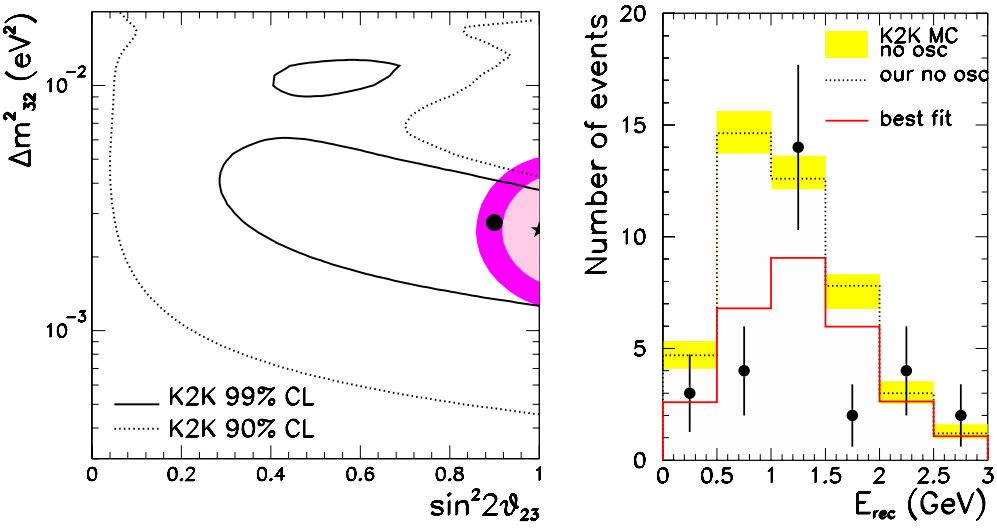

FIG. 1. $\nu_\mu \to \nu_\tau$ oscillation analysis of K2K data. On the left panel we show the allowed two degrees of freedom (DOFs), regions on $\Delta m^2, \sin^2 2\theta$ at 90% C.L. (solid) and 99% C.L. (dotted). The best fit point is marked with a thick dot. The shadowed regions are the 90, and 99% C.L. of the atmospheric neutrino analysis with the best point marked by a star. The right panel shows the spectrum of K2K events as a function of the reconstructed neutrino energy for the six bins used in the analysis. The data points are shown together with their statistical errors. The dotted histogram and the shaded boxes represent our prediction and the K2K Monte Carlo (MC) prediction in the absence of oscillations, respectively. The full line represents the expected distribution for the best fit point for $\nu_\mu \to \nu_\tau$ oscillations.

In each panel the displayed χ^2 has been marginalized with respect to the other two parameters. From the figure we see that the inclusion of K2K data in the analysis results in a reduction of the allowed range of Δm^2_{32} while the allowed range of θ_{23} is not modified. The reduction is more significant for the upper bound of Δm^2_{32} while the lower bound is slightly increased. More quantitatively, we find that the following ranges of parameters are allowed at 1σ (3σ) C.L. from this analysis:

$$(1.5)2.2 < \Delta m^2_{32}/10^{-3}\ \text{eV}^2 < 3.0(3.9),$$

$$(0.45)0.75 < \tan^2\theta_{23} < 1.3(2.3). \tag{9}$$

These ranges are consistent with the results from the two-neutrino oscillation analysis of K2K and atmospheric data in Ref. [32].

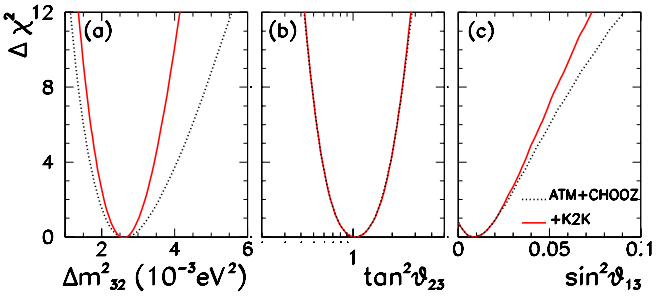

FIG. 2. 3ν oscillation analysis of the atmospheric, CHOOZ, and K2K data. The left, center, and right panels show the dependence of $\Delta\chi^2$ on Δm^2_{32}, $\tan^2\theta_{23}$, and $\sin^2\theta_{13}$ for the analysis of atmospheric, CHOOZ, and K2K data (full line) compared to the previous bound before the inclusion of K2K (dotted line). The individual 1σ (3σ) bounds in Eq. (9) can be read from the figure with the condition $\Delta\chi^2 \leqslant 1(9)$.

Concerning the "generic" 3ν mixing parameter θ_{13}, Eq. (6) shows that its effect on both the normalization and the shape of the ν_μ spectrum is further suppressed near maximal mixing by $\cos 2\theta_{23} \sim 0$. As a consequence, K2K alone does not provide any bound on θ_{13}. However, Fig. 2(c) illustrates how the inclusion of the long-baseline data results in a tightening of the bound on θ_{13} (at large C.L.) when combined with the atmospheric and CHOOZ data. This is an indirect effect due to the increase in the lower bound on Δm^2_{32}. In the favored range of Δm^2_{32}, the oscillating phase at CHOOZ is small enough so that it can be expanded and the oscillation probability of $\overline{\nu_e}$ depends quadratically on Δm^2_{32}. As a consequence the bound on the mixing angle from CHOOZ is a very sensitive function of the allowed values for Δm^2_{32}. The increase of the lower bound on Δm^2_{32} due to the inclusion of the K2K data leads to the tightening of the derived limit on θ_{13} at high C.L. From Fig. 2(c) and Table I we also see that the best fit point is not exactly at $\sin^2\theta_{13} = 0$, although this is not very statistically significant. This effect is due to the atmospheric neutrino data, in particular, to the slight excess of sub-GeV *e*-like events, which is better described with a nonvanishing value of θ_{13}.

B. Global analysis

We calculate the global χ^2 by fitting all the available data:

$$\begin{aligned}\chi^2_{\text{global}}(\Delta m^2_{21}, \Delta m^2_{32}, \theta_{12}, \theta_{23}, \theta_{13}) \\ = \chi^2_{\text{solar}}(\Delta m^2_{21}, \theta_{12}, \theta_{13}) + \chi^2_{\text{Kland}}(\Delta m^2_{21}, \theta_{12}, \theta_{13}) \\ + \chi^2_{\text{atm}}(\Delta m^2_{32}, \theta_{23}, \theta_{13}) + \chi^2_{\text{K2K}}(\Delta m^2_{32}, \theta_{23}, \theta_{13}) \\ + \chi^2_{\text{CHOOZ}}(\Delta m^2_{32}, \theta_{13}).\end{aligned} \tag{10}$$

The results of the global combined analysis are summarized

TABLE I. Minimum χ^2 values and best fit points for the 3ν oscillation analysis of atmospheric, CHOOZ, and K2K data.

	Atmos.	Atmos.+CHOOZ	Atmos.+CHOOZ+K2K
Data points	65	65+14=79	65+14+6=85
Δm^2_{32} (eV^2)	2.7×10^{-3}	2.55×10^{-3}	2.6×10^{-3}
$\tan^2\theta_{23}$	1	1	1
$\sin^2\theta_{13}$	0.015	0.009	0.009
$\chi^2_{\rm min}$	39.7	45.8	55.1

in Fig. 3 and Fig. 4 in which we show different projections of the allowed five-dimensional parameter space.

In Fig. 3 we plot the individual bounds on each of the five parameters derived from the global analysis (full line). To illustrate the impact of the K2K and KamLAND data we also show the corresponding bounds when K2K is not included in the analysis (dotted line) and when KamLAND is not included (dashed line). In each panel the displayed χ^2 has been marginalized with respect to the other four parameters. The subtracted minima for each of the curves are given in Table II.

Figure 3 illustrates that the dominant effects of including KamLAND are those derived in the two-neutrino oscillation analysis of solar and KamLAND data [16,17]: the determination that Δm^2_{21} (a) is in the LMA region and a very mild improvement of the allowed mixing angle θ_{12} (b). In other words, the inclusion of the 3ν mixing structure in the analysis of solar and KamLAND data does not affect the determination of these parameters once the additional angle θ_{13} is

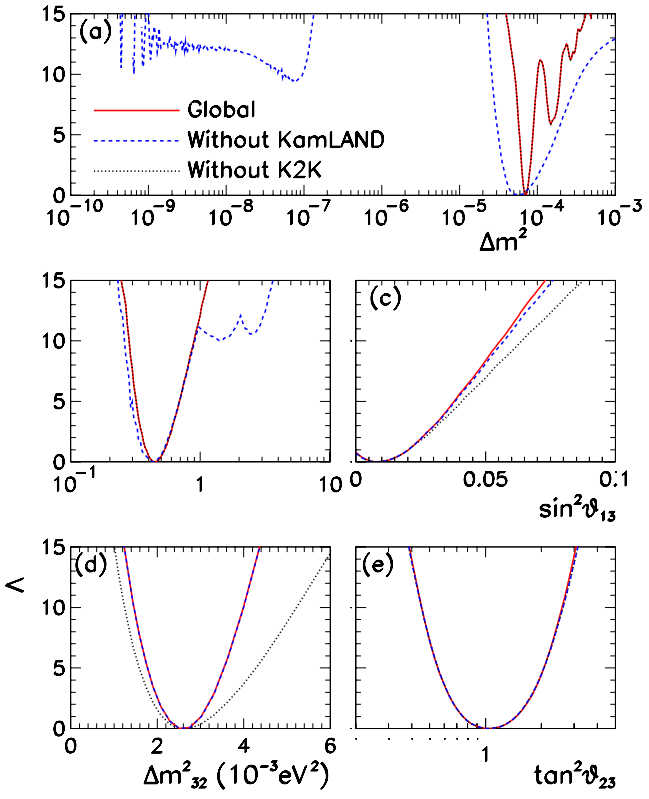

FIG. 3. Global 3ν oscillation analysis. Each panel shows the dependence of $\Delta\chi^2$ on each of the five parameters from the global analysis (full line) compared to the bound prior to the inclusion of the K2K (dotted line) and KamLAND data (dashed line). The individual 1σ (3σ) bounds in Eqs. (9), (11), and (12) can be read from the corresponding panel with the condition $\Delta\chi^2 \leqslant 1(9)$.

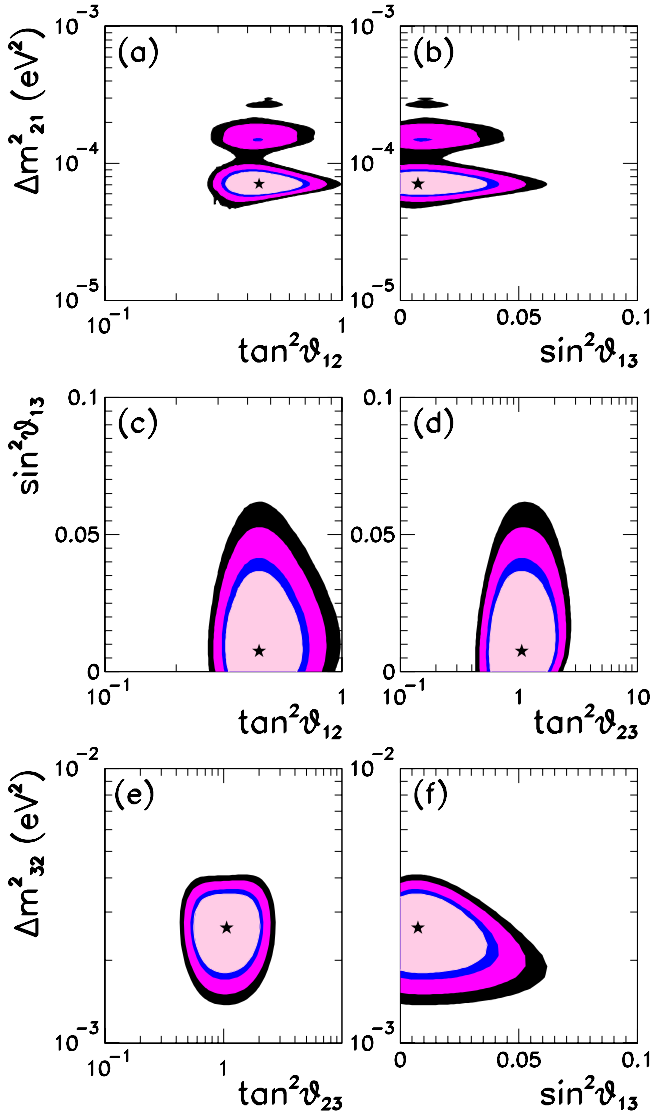

FIG. 4. Global 3ν oscillation analysis. Each panel shows two-dimensional projection of the allowed five-dimensional region after marginalization with respect to the three undisplayed parameters. The different contours correspond to the two-dimensional allowed regions at 90%, 95%, 99%, and 3σ C.L.

TABLE II. Minimum χ^2 values and best fit points for the global 3ν oscillation analysis.

	Global	Global-K2K	Global-KamLAND
Data points	178	172	165
Δm^2_{21} (eV^2)	7.1×10^{-5}	7.1×10^{-5}	5.8×10^{-5}
$\tan^2\theta_{12}$	0.45	0.45	0.45
Δm^2_{32} (eV^2)	2.6×10^{-3}	2.5×10^{-3}	2.6×10^{-3}
$\tan^2\theta_{23}$	1	1	1
$\sin^2\theta_{13}$	0.009	0.009	0.009
$\chi^2_{\rm min}$	136	127	130

bounded to be small. The slight tightening of the θ_{13} limit due to the inclusion of K2K data does not have any impact in the determination of the bounds on Δm^2_{21} and θ_{12}. Quantitatively, we find that the following ranges of parameters are allowed at 1σ (3σ) C.L. from this analysis:

$$(5.4)6.7<\Delta m^2_{21}/10^{-5}\ \text{eV}^2<7.7(10)$$

$$\text{and}\quad (14)<\Delta m^2_{21}/10^{-5}\ \text{eV}^2<(19),$$

$$(0.29)0.39<\tan^2\theta_{12}<0.51(0.82). \tag{11}$$

The range of Δm^2_{21} on the right of the first line in Eq. (11) correspond to solutions in the upper LMA island [see Fig. 4(a)]. At present the results of the solar and KamLAND analysis still allow for this ambiguity in the determination of Δm^2_{21} at C.L.$\gtrsim 2.5\sigma$. This reflects the departure from the parabolic (Gaussian) behavior of the Δm^2_{21} dependence of $\chi_{\rm global}$ and the presence of a second local minimum. With improved statistics KamLAND will be able to resolve this ambiguity [17,33].

Comparing the full line on the θ_{13} panel in Fig. 3(c) with the corresponding one in Fig. 2(c), we see that the inclusion of the solar+KamLAND data does have an impact on the allowed range of θ_{13}. However, a comparison of the full and dashed lines in Fig. 3(c) illustrates that the impact is due to the solar data. Equation (5) shows that a small θ_{13} does not significantly affect the shape of the measured spectrum at KamLAND. On the other hand, the overall normalization is scaled by $\cos^4\theta_{13}$, and this factor has the potential to introduce a non-negligible effect (in particular in the determination of the mixing angle θ_{12} [34]). Within its present accuracy, however, the KamLAND experiment cannot provide any further significant constraint on θ_{13}. Altogether, the derived bounds on θ_{13} from the global analysis are

$$\sin^2\theta_{13}<0.02(0.052) \tag{12}$$

at 1σ (3σ).

Finally, comparing Fig. 3(d) and Fig. 3(e) with the corresponding curves in Fig. 2(a) and Fig. 2(b), we see that the additional restriction on the possible range of θ_{13} imposed by the solar data does not quantitatively affect the dominant effect of the inclusion of K2K—the improved determination of Δm^2_{32}. Thus the allowed ranges of Δm^2_{32} and θ_{23} in Eq. (9) are valid for the global analysis as well.

The ranges in Eqs. (9), (11), and (12) are not independent. In Fig. 4 we plot the correlated bounds from the global analysis for each pair of parameters. The regions in each panel are obtained after marginalization of $\chi^2_{\rm global}$ in Eq. (10) with respect to the three undisplayed parameters. The different contours correspond to regions defined at 90%, 95%, 99%, and 3σ C.L. for two DOFs ($\Delta\chi^2 = 4.61, 5.99, 9.21, 11.83$), respectively. From the figure we see that the strongest correlation appears between θ_{13} and Δm^2_{32} as a reflection of the CHOOZ bound.

In general, because of the correlations, the ranges in Eqs. (9), (11), and (12) cannot be directly used in deriving the corresponding entries in the U mixing matrix, as we discuss next.

C. Determination of the leptonic mixing matrix

We describe in this section our procedure to consistently derive the allowed ranges for the magnitude of the entries of the leptonic mixing matrix. We start by defining the mass-marginalized χ^2 function:

$$\chi^2_{\rm mix,global}(\theta_{12},\theta_{23},\theta_{13}) = \min_{(\Delta m^2_{21},\Delta m^2_{32})} \chi^2_{\rm global}(\Delta m^2_{21},\Delta m^2_{32},\theta_{12},\theta_{23},\theta_{13}). \tag{13}$$

We study the variation of $\chi^2_{\rm mix,global}$ as function of each of the mixing combinations in U as follows. For a given magnitude $\overline{U_{ij}}$ of the entry $U(i,j)$, we define $\chi^2(\overline{U_{i,j}})$ as the minimum value of $\chi^2_{\rm mix,global}(\theta_{12},\theta_{23},\theta_{13})$ with the condition $|U(i,j)(\theta_{12},\theta_{23},\theta_{13})| = \overline{U_{i,j}}$. In this procedure the phase δ is allowed to vary freely between 0 and π. The allowed range of the magnitude of the entry ij at a given C.L. is then defined as the values $\overline{U_{i,j}}$ satisfying

$$\chi^2(\overline{U_{i,j}}) - \chi^2_{\rm global,min} \leqslant \Delta\chi^2(\text{C.L., one DOF}), \tag{14}$$

with $\chi^2_{\rm global,min} = 136$. This is equivalent to having done the full analysis in terms of the independent matrix elements—of which, in the hierarchical approximation, only three are experimentally accessible at present (and can be chosen, for instance, to be $|U_{e2}|$, $|U_{e3}|$, and $|U_{\mu 3}|$)—and find the allowed magnitude of each $|U_{ij}|$ by marginalization of

$$\chi^2_{\rm mix,global}(|U_{e2}|,|U_{e3}|,|U_{\mu 3}|), \tag{15}$$

with the use of unitarity relations and allowing a free relative phase δ.

With this procedure we derive the following 90% (3σ) C.L. limits on the magnitude of the elements of the complete matrix:

$$U=\begin{pmatrix} (0.73)0.79 \text{ to } 0.86(0.88) & (0.47)0.50 \text{ to } 0.61(0.67) & 0 \text{ to } 0.16(0.23) \\ (0.17)0.24 \text{ to } 0.52(0.57) & (0.37)0.44 \text{ to } 0.69(0.73) & (0.56)0.63 \text{ to } 0.79(0.84) \\ (0.20)0.26 \text{ to } 0.52(0.58) & (0.40)0.47 \text{ to } 0.71(0.75) & (0.54)0.60 \text{ to } 0.77(0.82) \end{pmatrix}. \quad (16)$$

By construction the derived limits in Eq. (16) are obtained under the assumption of the matrix U being unitary. In other words, the ranges in the different entries of the matrix are correlated due to the fact that, in general, the result of a given experiment restricts a combination of several entries of the matrix, as well as due to the constraints imposed by unitarity. As a consequence, choosing a specific value for one element further restricts the range of the others.

D. Δm^2_{21} oscillations at future long-baseline experiments

In general, correlations between the allowed ranges of the parameters have to be considered when deriving the present bounds for any quantity involving two or more parameters. This is the case, for example, when predicting the allowed range of *CP* violation at future experiments as discussed in Ref. [35].

Here we explore the possible size of effects associated with Δm^2_{21} oscillations (both *CP* violating and *CP* conserving) at future long-baseline experiments to be performed either with conventional superbeams [36] (''conventional'' meaning from the decay of pions generated from a proton beam dump) or at a neutrino factory [37] with neutrino beams from muon decay in muon storage rings.

The ''golden'' channel at these facilities involves the observation of either ''wrong-sign'' muons due to $\nu_e \to \nu_\mu$ (or $\bar{\nu}_e \to \bar{\nu}_\mu$) oscillations at a neutrino factory or the detection of electrons (positrons) due to $\nu_\mu \to \nu_e$ ($\bar{\nu}_\mu \to \bar{\nu}_e$) at conventional superbeams. In either case, the relevant oscillation probabilities in vacuum are accurately given by [38,39]

$$P_{\nu_e\nu_\mu} = s^2_{23}\sin^2 2\theta_{13}\sin^2\left(\frac{\Delta m^2_{32}L}{4E}\right) + c^2_{23}\sin^2 2\theta_{12}\left(\frac{\Delta m^2_{21}L}{4E}\right)^2 + \tilde{J}\cos\left(\delta + \frac{\Delta m^2_{32}L}{4E}\right)\left(\frac{\Delta m^2_{21}L}{4E}\right)\sin\left(\frac{\Delta m^2_{32}L}{4E}\right) = P^{\rm atm} + P^{\rm sol} + P^{\rm inter}, \quad (17)$$

with $\tilde{J} = c_{13}\sin 2\theta_{12}\sin 2\theta_{13}\sin 2\theta_{23}$. $P^{\rm sol}$ contains the contribution to the probability due to longer-wavelength oscillations while $P^{\rm inter}$ gives the interference between the longer- and shorter-wavelength oscillations and contains the information on the *CP*-violating phase δ. In order to quantify the present bounds on these contributions, we factorize the baseline and energy independent parts as

$$P^{\rm sol} = (F^{\rm sol})^2\left(\frac{L}{4E}\right)^2,$$

$$P^{\rm inter} = F^{\rm inter}\cos\left(\delta - \frac{\Delta m^2_{32}L}{4E}\right)\sin\left(\frac{\Delta m^2_{32}L}{4E}\right)\left(\frac{L}{4E}\right),$$

$$F^{\rm sol} = c_{23}\sin 2\theta_{12}\Delta m^2_{21},$$

$$F^{\rm inter} = c_{13}\sin 2\theta_{12}\sin 2\theta_{13}\sin 2\theta_{23}\Delta m^2_{21}. \quad (18)$$

For very long baselines, for which the presence of matter cannot be neglected, the expressions above for $F^{\rm sol}$ and $F^{\rm inter}$ still hold as the coefficients of the dominant contributions to the probabilities in the expansion in the small parameters θ_{13} and Δm^2_{21} [38,39].

We show in Fig. 5 the present bounds on the coefficients $F^{\rm sol}$ and $F^{\rm inter}$. In general, the dependence on Δm^2_{32} of the interference term cannot be factorized because, depending on the considered baseline and energy, the oscillating phase with Δm^2_{32} may not be small enough to be expanded. For this reason we show in Fig. 5(b) the two-dimensional allowed region of $F^{\rm inter}$ versus Δm^2_{32}. In the figure we mark with a star the best value for $F^{\rm inter}$ as obtained from this analysis, which is not vanishing due to the small but nonzero best fit value of $\sin\theta_{13}$. This is, however, not statistically significant as $F^{\rm inter}=0$ is at $\Delta\chi^2 = 0.9$. The negative slope in the upper part of the 90% and 95% C.L. regions in Fig. 5(b) is a reflection of the anticorrelation between the Δm^2_{32} and $\sin^2\theta_{13}$ constraints from the CHOOZ experiment [see Fig. 4(f)].

From this study we find the following 1σ (3σ) (one DOF) bounds:

$$F^{\rm sol}/(10^{-5}\ \text{eV}^2) = 4.6 \pm 0.6 \ \ (4.6^{+2.1}_{-1.6} \text{ and } 9.5^{+3.5}_{-2.0}), \quad (19)$$

$$0 < F^{\rm inter}/(10^{-5}\ \text{eV}^2) < 1.9(5.5), \quad (20)$$

where the bounds on $F^{\rm inter}$ are shown for the best fit value of $\Delta m^2_{32} = 0.0026\ \text{eV}^2$. The larger values for the 3σ range in Eq. (19) and $F^{\rm inter}$ correspond to solutions of the solar

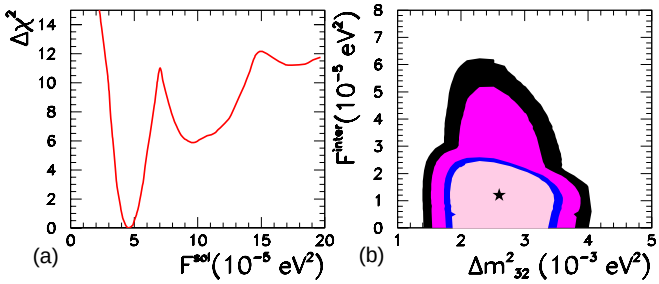

FIG. 5. (a) Dependence of $\Delta\chi^2$ on $F^{\rm sol}$. (b) Allowed regions of $F^{\rm inter}$ versus Δm^2_{32} at 90%, 95%, 99% and 3σ. The best value is marked with a star.

+KamLAND analysis lying in the higher-Δm^2_{21} island [see Fig. 4(a) and the discussion below Eq. (11)].

IV. SUMMARY AND CONCLUSIONS

We have presented the results of an updated global analysis of solar, atmospheric, reactor, and long-baseline neutrino data in the context of three-neutrino oscillations, placing special emphasis on the impact of the recent long-baseline ν_μ disappearance data from the K2K experiment and reactor $\bar{\nu}_e$ disappearance from the KamLAND experiment. We find that the dominant effect of the inclusion of the K2K and KamLAND data is the reduction of the allowed ranges of Δm^2_{32} and Δm^2_{21}, respectively, while the impact on the mixing angles θ_{23} and θ_{12} is marginal. The increase of the lower bound on Δm^2_{32} due to the inclusion of the K2K data leads also to a slight tightening of the derived limit on θ_{13} at high C.L. Our results on the individual allowed ranges for the oscillation parameters are given in Eqs. (9), (11), and (12) and graphically displayed in Fig. 3. The correlations between the derived bounds are illustrated in Fig. 4. As an outcome of the analysis, we have presented in Eq. (16) our up-to-date best determination of the magnitude of the elements of the complete leptonic mixing matrix. Finally, we have quantified the allowed contribution of Δm^2_{21} oscillations to *CP*-odd and *CP*-even observables at future long-baseline experiments with results presented in Fig. 5 and Eqs. (19) and (20).

ACKNOWLEDGMENTS

We are particularly indebted to T. Kobayashi for providing us with information and clarifications about the K2K analysis. We thank M. Maltoni for many useful discussions and for his collaboration on the atmospheric neutrino analysis during the early stages of this work. This work was supported in part by the National Science Foundation Grant No. PHY0098527. C.P.G. acknowledges support from NSF Grant No. PHY0070928. M.C.G.-G. is also supported by Spanish Grants No. FPA-2001-3031 and No. CTIDIB/2002/24.

APPENDIX: ANALYSIS OF K2K DATA

In this appendix we describe our calculation of the K2K spectrum and our statistical analysis of the K2K data [13].

We use in our statistical analysis the K2K data on the spectrum of single-ring μ-like events. K2K present their results as the number of observed events as a function of the reconstructed neutrino energy. The reconstructed neutrino energy is determined from the observed μ energy in the event, E_μ, and its scattering angle with respect to the incoming beam direction, $\cos\theta_\mu$, as

$$E_{\rm rec}=\frac{m_N E_\mu - m_\mu^2/2}{m_N - E_\mu + p_\mu \cos\theta_\mu}, \tag{A1}$$

where m_N is the nucleon mass. In Fig. 1 we show their data binned in five 0.5 GeV bins with $0<E_{\rm rec}<2.5$ plus one bin containing all events above 2.5 GeV. The total sample corresponds to 29 events. In the absence of oscillations, 44 events were expected.

For QE events, $\nu_\mu n\to\mu p$, and assuming perfect E_μ and $\cos\theta_\mu$ determination, $E_{\rm rec}=E_\nu$. Experimental energy and angular resolution, nuclear effects, and, more importantly, the contamination from non-QE (NQE) events, $\nu_\mu N\to\mu X$, in the sample, result in important deviations of the defined $E_{\rm rec}$ from the *real* E_ν. From simple kinematics one finds that in NQE events there is a shift in the reconstructed neutrino energy with respect to the true neutrino energy:

$$E_{\rm rec}=E_\nu\left[1+\frac{M_X^2-m_N^2}{m_N E_\mu - m_\mu^2/2}\right]^{-1}<E_\nu, \tag{A2}$$

where M_X is the invariant mass of the hadronic system produced together with the muon in the ν_μ interaction. At the K2K energies the most important NQE contamination comes from single pion production, which occurs via the Δ resonance. At the largest energies there is a small contribution from deep inelastic scattering.

Thus in general the observed spectrum of single-ring μ-like events in K2K can be obtained as [40]

$$\begin{aligned} N^{\rm th}(E_{\rm rec}) = N_{\rm norm}\int \Phi_{\rm SK}(E_\nu) P_{\mu\mu}(E_\nu) \\ \times[\sigma_{\rm QE}(E_\nu)\epsilon_{\rm QE}^{1R_\mu}(E_\nu) r_{\rm QE}(E_\nu,E_{\rm rec}) \\ + f_{\rm NQE}\sigma_{\rm NQE}(E_\nu)\epsilon_{\rm NQE}^{1R_\mu}(E_\nu) r_{\rm NQE}(E_\nu,E_{\rm rec})]dE_\nu, \end{aligned} \tag{A3}$$

where $\Phi_{\rm SK}(E_\nu)$ is the expected ν_μ spectrum at the SK site in the absence of oscillations. $P_{\mu\mu}(E_\nu)$ is the survival probability of ν_μ for a given set of oscillation parameters. $f_{\rm NQE}=0.93$ is the rescaling factor of the expected contamination from NQE events as obtained from MC simulation by the K2K Collaboration [13]. $\sigma_{\rm QE(NQE)}(E_\nu)$ are the neutrino interaction cross sections. $\epsilon^{1R_\mu}_{\rm QE(NQE)}$ are the detection efficiencies for one-ring μ-like events at SK. $r_{\rm QE(NQE)}(E_\nu,E_{\rm rec})$ are the functions relating the reconstructed energy and the true neutrino energy. $N_{\rm norm}$ is the normalization factor, which is chosen so that in the absence of oscillations the total integral gives 44 events.

In our calculation we use the neutrino spectrum $\Phi_{\rm SK}$ as provided by the K2K Collaboration [40,41]. This flux was estimated from the flux measured in the near detector by multiplying it by a MC simulated ratio of the fluxes between the near and far detectors. We further assume that the detection efficiencies for one-ring μ-like events at SK are the same for the K2K analysis as for the atmospheric neutrino analysis (further details and references can be found in Ref. [23]).

At present there is not enough information from the K2K Collaboration on the $r_{\rm QE(NQE)}(E_\nu,E_{\rm rec})$ functions. In our calculation we have used a *physically motivated* form for those functions. We include in the functions $r_{\rm QE(NQE)}(E_\nu,E_{\rm rec})$ the dominant effect in the misreconstruction of the neutrino en-

ergy: the shift in the reconstructed neutrino energy due to the different kinematics of the NQE events as described by Eq. (A2). We also include the (subdominant) effects due to the experimental energy and angular resolutions, which smear the measured muon energy E_μ and angle θ_μ around their true values E'_μ and θ'_μ:

$$r_{\rm QE}(E_\nu,E_{\rm rec})=\frac{1}{\sigma_{\rm QE}(E_\nu)}\int dE'_\mu dE_\mu d\theta \frac{d\sigma_{\rm QE}(E_\nu,E'_\mu)}{dE'_\mu} \times {\rm Res}_E(E_\mu-E'_\mu){\rm Res}_\theta(\theta_\mu-\theta'_\mu) \times \delta(E_\nu-E'_{\rm rec}),$$

$$r_{\rm NQE}(E_\nu,E_{\rm rec})=\frac{1}{\sigma_{\rm NQE}(E_\nu)}\int dE'_\mu dE_\mu d\theta dM_X \times \frac{d\sigma_{\rm NQE}(E_\nu,E'_\mu,M_X)}{dE'_\mu dM_X}{\rm Res}_E(E_\mu-E'_\mu) \times {\rm Res}_\theta(\theta_\mu-\theta'_\mu) \times \delta\left(E_\nu-E'_{\rm rec}\left[1+\frac{M_X^2-m_N^2}{m_N E'_\mu-m_\mu^2/2}\right]^{-1}\right), \tag{A4}$$

where

$$E'_{\rm rec}=E_{\rm rec}\frac{m_N E_\mu-m_\mu^2/2}{m_N-E_\mu+p_\mu\cos\theta'_\mu}\,\frac{m_N-E'_\mu+p'_\mu\cos\theta_\mu}{m_N E'_\mu-m_\mu^2/2},$$

$${\rm Res}_E(E'_\nu-E_\nu)=\frac{1}{\sqrt{2\pi}\sigma_E}e^{-(1/2)(E_\mu-E'_\mu)^2/\sigma_E^2},$$

$${\rm Res}_\theta(\theta'_\nu-\theta_\nu)=\frac{1}{\sqrt{2\pi}\sigma_\theta}e^{-(1/2)(\theta_\mu-\theta'_\mu)^2/\sigma_\theta^2}. \tag{A5}$$

Following the SK data [2] we use an energy resolution for the muons of $\sigma_E/E_\mu=3\%$ and an angular resolution $\sigma_\theta=3^\circ$ (see also Ref. [42] for further details). Notice that in the expressions above the true angle of the muon, θ'_μ, is not an independent variable but is related by the kinematics of the process to the initial neutrino energy E_ν, the final muon energy E'_μ, and the invariant mass of the hadronic system, M_X. The final result for the number of expected events in each $E_{\rm res}$ bin is obtained by substituting Eqs. (A4) and (A5) into Eq. (A3) and numerically integrating for the kinematical variables in the corresponding range of $E_{\rm res}$. In this procedure the only free parameter to adjust is the overall normalization. The shape of the spectrum is then fully determined.

In order to verify the quality of our simulation we compare our predictions for the energy distribution of the events with the Monte Carlo simulations of the K2K Collaboration in absence of oscillation. In Fig. 1 we show our predictions superimposed on those from the experimental Monte Carlo calculations (obtained from Fig. 2 in Ref. [13]), both normalized to the 44 expected events in the absence of oscillations. The boxes for the MC prediction represent the systematic error bands. We can see that the agreement in the shape of the spectrum is very good.

In our statistical analysis of the K2K data we use Poisson statistics as required given the small number of events. We include the systematic uncertainties associated with the determination of the neutrino energy spectrum in the near detector (ND), the model dependence of the size of the NQE contamination parameter $f_{\rm NQE}$, the near/far extrapolation (F/N), and the overall flux normalization (nor) [40,41]. The errors on the first three items depend on energy and have correlations among the different energy bins. We account for all these effects by using the χ^2 function [32,40,41]:

$$\chi^2_{\rm K2K}=\min_f\left[2\sum_{i=1}^{6}\left(\overline{N}_i^{\rm theor}-N_i^{\rm expt}-N_i^{\rm expt}\ln\frac{\overline{N}_i^{\rm theor}}{N_i^{\rm exp}}\right) +\sum_{j,k=1}^{6} f_j^{F/N}(\rho^{F/N})^{-1}_{ij}f_j^{F/N} +\sum_{j,k=1}^{7} f_j^{\rm ND,NQE}(\rho^{\rm ND,NQE})^{-1}_{ij}f_j^{\rm ND,NQE}+f^{\rm nor2}\right], \tag{A6}$$

where $\overline{N}_i^{\rm theor}=N_i^{\rm theor}(1+f_i^{\rm F/N}\sigma_i^{\rm F/N}+f_i^{\rm ND}\sigma_i^{\rm ND}+f^{\rm NQE}\sigma_i^{\rm NQE}+f^{\rm nor}\sigma^{\rm nor})$. By $\min_f$ we denote the minimization with respect to the systematic shift parameters (or pulls [32]) $f^{\rm F/N}_{i=1,6}$, $f^{\rm ND}_{i=1,6}$, $f^{\rm NQE}$, and $f^{\rm nor}$. We use the systematic errors and their correlations as provided by the K2K Collaboration [13,40,41]. For instance,

$$\sigma^{\rm nor}=5\%,$$

$$\sigma_i^{\rm F/N}=2.5\%,4.3\%,6.5\%,10.4\%\ \ 11.1\%,12.2\%,$$

$$\sigma_i^{\rm ND}=49\%,7.1\%,0\%,7.1\%\ \ 8.4\%,11.1\%,$$

$$\sigma_i^{\rm NQE}=13\%,8.9\%,6\%,3.8\%\ \ 3.\%,5.5 \tag{A7}$$

for $i=1,\ldots,6$, respectively.

Thus in our analysis we use both the shape and the normalization of the 29 single-ring μ-like events. In their analysis, the K2K Collaboration use only the spectrum shape (but not the normalization) of the 29 single-ring μ-like events plus the overall normalization of their total sample of fully contained events (a total of 56). We cannot use the normalization from the additional 27 events in the lack of more detailed information from the K2K Collaboration on the efficiencies for multiring events. Nevertheless, as described in Sec. III A, the results of our oscillation analysis are in good agreement with those from the K2K analysis.

[1] SuperKamiokande Collaboration, M. Shiozawa, in XXth International Conference on Neutrino Physics and Astrophysics, Munich, 2002, http://neutrino2002.ph.tum.de
[2] Y. Fukuda *et al.*, Phys. Lett. B **433**, 9 (1998); **436**, 33 (1998); **467**, 185 (1999); Phys. Rev. Lett. **82**, 2644 (1999).
[3] MACRO Collaboration, M. Ambrosio *et al.*, Phys. Lett. B **517**, 59 (2001); M. Goodman, in XXth International Conference on Neutrino Physics and Astrophysics, Munich, 2002, http://neutrino2002.ph.tum.de
[4] SOUDAN-2 Collaboration, D.A. Petyt, Nucl. Phys. B (Proc. Suppl.) **110**, 349 (2002).
[5] Q.R. Ahmad *et al.*, Phys. Rev. Lett. **87**, 071301 (2001); *ibid.* **89**, 011301 (2002).
[6] Super-Kamiokande Collaboration, S. Fukuda *et al.*, Phys. Lett. B **539**, 179 (2002).
[7] B.T. Cleveland *et al.*, Astrophys. J. **496**, 505 (1998).
[8] J.N. Abdurashitov *et al.*, J. Exp. Theor. Phys. **95**, 181 (2002).
[9] GALLEX Collaboration, W. Hampel *et al.*, Phys. Lett. B **447**, 127 (1999).
[10] T. Kirsten, talk at the XXth International Conference on Neutrino Physics and Astrophysics (NU2002), Munich, 2002; M. Altmann *et al.*, Phys. Lett. B **490**, 16 (2000); GNO Collaboration, E. Bellotti *et al.*, in *Neutrino 2000*, Proceedings of the XIXth International Conference on Neutrino Physics and Astrophysics, 2000, edited by J. Law, R.W. Ollerhead, and J.J. Simpson [Nucl. Phys. B (Proc. Suppl.) **91,** 44 2001].
[11] Y. Fukuda *et al.*, Phys. Rev. Lett. **77**, 1683 (1996).
[12] J.N. Bahcall, N.A. Bahcall, and G. Shaviv, Phys. Rev. Lett. **20**, 1209 (1968); J.N. Bahcall and R. Davis, Science **191**, 264 (1976).
[13] M.H. Ahn *et al.*, Phys. Rev. Lett. **90**, 041801 (2003).
[14] KamLAND Collaboration, K. Eguchi *et al.*, Phys. Rev. Lett. **90**, 021802 (2003).
[15] J.N. Bahcall, M.C. Gonzalez-Garcia, and C. Pena-Garay, J. High Energy Phys. **07**, 054 (2002).
[16] J.N. Bahcall, M.C. Gonzalez-Garcia, and C. Pena-Garay, J. High Energy Phys. **02**, 009 (2003).
[17] G.L. Fogli, E. Lisi, A. Marrone, D. Montanino, A. Palazzo, and A.M. Rotunno, Phys. Rev. D **67**, 073002 (2003); M. Maltoni, T. Schwetz, and J.W.F. Valle, *ibid.* **67**, 093003 (2003); P. Creminelli, G. Signorelli, and A. Strumia, J. High Energy Phys. **05**, 052 (2001); A. Bandyopadhyay, S. Choubey, R. Gandhi, S. Goswami, and D.P. Roy, Phys. Lett. B **559**, 121 (2003); P.C. de Holanda and A.Y. Smirnov, J. Cosmol. Astropart. Phys. **02**, 001 (2003); H. Nunokawa, W.J. Teves, and R. Zukanovich Funchal, Phys. Lett. B **562**, 28 (2003); A.B. Balantekin and H. Yuksel, J. Phys. G **29**, 665 (2003); V. Barger and D. Marfatia, Phys. Lett. B **555**, 144 (2003); P. Aliani, V. Antonelli, M. Picariello, and E. Torrente-Lujan, hep-ph/0212212.
[18] For a recent review, see M.C. Gonzalez-Garcia and Y. Nir, Rev. Mod. Phys. **75**, 345 (2003).
[19] B. Pontecorvo, Zh. Éksp. Teor. Fiz. **33**, 549 (1957) [Sov. Phys. JETP **6**, 429 (1958)]; Z. Maki, M. Nakagawa, and S. Sakata, Prog. Theor. Phys. **28**, 870 (1962); M. Kobayashi and T. Maskawa, *ibid.* **49**, 652 (1973).
[20] Particle Data Group, D.E. Groom *et al.*, Eur. Phys. J. C **15**, 1 (2000).
[21] S.M. Bilenky, J. Hosek, and S.T. Petcov, Phys. Lett. B **94**, 495 (1980).
[22] M. Apollonio *et al.*, Phys. Lett. B **466**, 415 (1999).
[23] N. Fornengo, M.C. Gonzalez-Garcia, and J.W.F. Valle, Nucl. Phys. **B580**, 58 (2000); M.C. Gonzalez-Garcia, H. Nunokawa, O.L.G. Peres, and J.W.F. Valle, *ibid.* **B543**, 3 (1999); M.C. Gonzalez-Garcia, H. Nunokawa, O.L.G. Peres, T. Stanev, and J.W.F. Valle, Phys. Rev. D **58**, 033004 (1998).
[24] M.C. Gonzalez-Garcia, M. Maltoni, C. Pena-Garay, and J.W.F. Valle, Phys. Rev. D **63**, 033005 (2001).
[25] M.C. Gonzalez-Garcia and M. Maltoni, Eur. Phys. J. C **26**, 417 (2003).
[26] J.N. Bahcall, M.H. Pinsonneault, and S. Basu, Astrophys. J. **555**, 990 (2001).
[27] R. Foot, R.R. Volkas, and O. Yasuda, Phys. Rev. D **58**, 013006 (1998); O. Yasuda, *ibid.* **58**, 091301 (1998); E.Kh. Akhmedov, A. Dighe, P. Lipari, and A.Yu. Smirnov, Nucl. Phys. **B542**, 3 (1999).
[28] E. Lisi and D. Montanino, Phys. Rev. D **56**, 1792 (1997).
[29] A.M. Dziewonski and D.L. Anderson, Phys. Earth Planet. Inter. **25**, 297 (1981).
[30] S.M. Bilenky, D. Nicolo, and S.T. Petcov, Phys. Lett. B **538**, 77 (2002); S.T. Petcov and M. Piai, *ibid.* **533**, 94 (2002).
[31] I. Mocioiu and R. Shrock, J. High Energy Phys. **11**, 050 (2001).
[32] G.L. Fogli, E. Lisi, A. Marrone, and D. Montanino, Phys. Rev. D **67**, 093006 (2003).
[33] J.N. Bahcall and C. Pena-Garay, hep-ph/0305159.
[34] M.C. Gonzalez-Garcia and C. Peña-Garay, Phys. Lett. B **527**, 199 (2002).
[35] G.L. Fogli, G. Lettera, E. Lisi, A. Marrone, A. Palazzo, and A. Rotunno, Phys. Rev. D **66**, 093008 (2002).
[36] B. Richter, hep-ph/0008222; V. Barger, S. Geer, R. Raja, and K. Whisnant, Phys. Rev. D **63**, 113011 (2001); J.J. Gomez-Cadenas *et al.*, hep-ph/0105297; Y. Itow *et al.*, hep-ex/0106019; M.V. Diwan *et al.*, Phys. Rev. D **68**, 012002 (2003).
[37] S. Geer, Phys. Rev. D **57**, 6989 (1998). A. De Rujula, M.B. Gavela, and P. Hernandez, Nucl. Phys. **B547**, 21 (1999); J. J. Gomez-Cadenas and D. A. Harris, Report No. FERMILAB-PUB-02-044-T.
[38] A. Cervera, A. Donini, M.B. Gavela, J.J. Gomez Cadenas, P. Hernandez, O. Mena, and S. Rigolin, Nucl. Phys. **B579**, 17 (2000).
[39] H.W. Aagluer and K.H. Shwarzer, Z. Phys. C **40**, 1988 (273); M. Freund, Phys. Rev. D **64**, 053003 (2001); K. Kimura, A. Takamura, and H. Yokomakura, *ibid.* **66**, 073005 (2002).
[40] T. Kobayashi, in Proceedings of the 4th International Workshop on Neutrino Factories Based on Muon Storage Rings, London, 2002, http://www.hep.ph.ic.ac.uk/NuFact02
[41] K2K Collaboration (private communication).
[42] A. Blondel, M. Campanelli, and M. Fechner, in Proceedings of the 4th International Workshop on Neutrino Factories Based on Muon Storage Rings, London, 2002, http://www.hep.ph.ic.ac.uk/NuFact02